Design an optimal robust integral signum of the error controller for electrical vehicle based on salp swarm optimization algorithm

Arkan A. Jassim[1], Ekhlas H. Karam[2], Mohammed Moanes E. Ali[1]
[1]Department of Electrical Engineering, University of Technology, Baghdad, Iraq
[2]Department of Computer Engineering, Mustansiriyah University, Baghdad, Iraq

Article Info

ABSTRACT

The electric vehicle (EV) has nowadays become a suitable alternative to clean and sustainable energy emissions in transportation, so researchers have become interested in modeling and controlling the electric vehicle.in this paper, an optimal robust integral signum of the error (ORISE) controller is designed to control the actuator speed of an electric vehicle. The actuator type of this vehicle is three-phase induction motor (IM). By reducing the discrepancy between the desired and actual output, the standard salp swarm algorithm (SSA) is utilized to find the optimal suggested ORISE parameter. The suggested controller tested by different desired velocity trajectory. Simulation results demonstrate that the ORISE have high performance, fast and accurate tracking for the EV speed, compare with PID controller that the output speed suffer from chattering and has higher oscillation. In particular, the SSA-based ORISE controller is superior to the proportional-integral-derivative (PID)-based SSA method in terms of no steady-state error and smallest overshoot (0.002% with ORISE while 0.05% with PID) prevention for electric vehicle (EV) speed despite the better results of settling time and rising time obtained in PID (1.532s and 0.785s) respectively while these values were (1.574s and 1.915s) respectively, in ORISE. The MATLAB (R2020a)/Simulink environment is used for all projects.

Corresponding Author:

Arkan A. Jassim
Department of Electrical Engineering, University of Technology
Baghdad, Iraq
Email: arkan199328@gmail.com

1. INTRODUCTION

The automotive sector, and particularly the electric vehicle (EV) sector, is having a period of significant redeployment. With so many advantages that electric vehicles (EVs) provide, many firms have begun to base their new automobile models on electricity. An eco-friendly framework that combines zero emissions, excellent power efficiency, and minimum noise pollution underpins the dominance of EVs in the transportation sector [1], [2]. The usage of EVs lessens a country's dependency on foreign oil imports, and on a personal level, they are more cost-effective than gasoline due to the low maintenance needs of electric motors and low energy prices [3]. Tax breaks and bonuses help to significantly lower the cost of operating an EV. Due to their integrated operation with sources of clean energy, electric vehicles' advantages on economic matters are increased even more [4] as well as the potential to offer supplementary services to the grid [5], [6].

Due to their excellent combination of affordability, dependability, and performance, induction motors are currently the most popular alternating current or AC equipment. Several methods, ranging from

the low-cost constant voltage/frequency ratio strategy to the complex sensorless control schemes, can be used to manage torque in induction motors. These effective strategies are being used in electric automobiles [7]. The rapid development of power electronics and micro-computing has led to substantial advancements in the control of AC electric machinery as well as in real-time implantation applications facilities. Induction motors (IMs), in particular, have a number of built-in benefits, including ease of use, dependability, affordability, and nearly maintenance-free electrical drives [8]. However, since they exhibit large nonlinearities and several characteristics, most notably the rotor resistance, vary depending on operating conditions, controlling high dynamic performance in industrial applications continues to be a difficult task. However, due to its simplicity of operation and the fact that torque and flux were naturally decoupled and could be controlled separately by the torque and the flux, both of which produced current, the direct current machine (DC) over time evolved into the only electromechanical source for variable speed applications [8]–[10].

The robust controller is one of the numerous types of techniques that are used to control the induction motor. A system's capacity to reject shocks or uncertainties in order to behave as closely as feasible to its normal operation is referred to as robust control. A robust control system maintains a certain level of stability or performance in the face of external disturbances. When designing and analyzing control systems, robustness is an important quality that must be considered [11].

Previously, there were many research that used robust control approaches for controlling the induction motor or the electrical vehicle such as, in 2015, Nasri *et al.* [12] introduce in their research a new approach on the sliding mode control that can be applied on four electric vehicle independent wheels. In 2020, Pourseif and Mohajeri [13] presented that the permanent magnet synchronous motor is controlled using robust control approaches. This method is more effective since it performs well even when the vehicle's load torque disturbs it, as well as despite measurement noise, changes in system parameters, and high-frequency uncertainty in both structured and unstructured forms. The control goal is to regulate and maintain the vehicle's speed and motor torque in the intended references for the driver. In 2021, Zand *et al.* [14] explained the super twisting sliding mode control (STSMC) that is being given is intended for direct torque and flux control for three-phase induction machine speed control. In order to ensure the stability of the drive control system while it is subject to disturbances, Lyapunov's theory has also been utilized. In 2021, Jin *et al.* [15] offers a constrained robust H∞ controller architecture for an in-wheel independent drive active suspension system for electric vehicles while taking control constraints and parameter volatility into mind. Compared with earlier research. The induction motor of the electrical vehicle is controlled by an optimal, robust integral signum of the error controller, the parameters of which are determined by SSA.

This paper is structured as: i) The modeling of electric vehicle is presented in section 2; ii) In section 3, the details of the suggested ORISE controller are given; iii) Section 4 presents the salp swarm optimization methodologies; iv) The section devoted to presenting the results obtained in section 5; and v) A conclusion is provided in section 6.

2. MODELING OF ELECTRIC TRACTION SYSTEM ELEMENTS

Figure 1 shows electric traction system with induction motor (IM) and voltage inverter [16]. The electric traction system consists of several key components, including an IM and a voltage inverter. The following subsection provides a detailed illustration of each component.
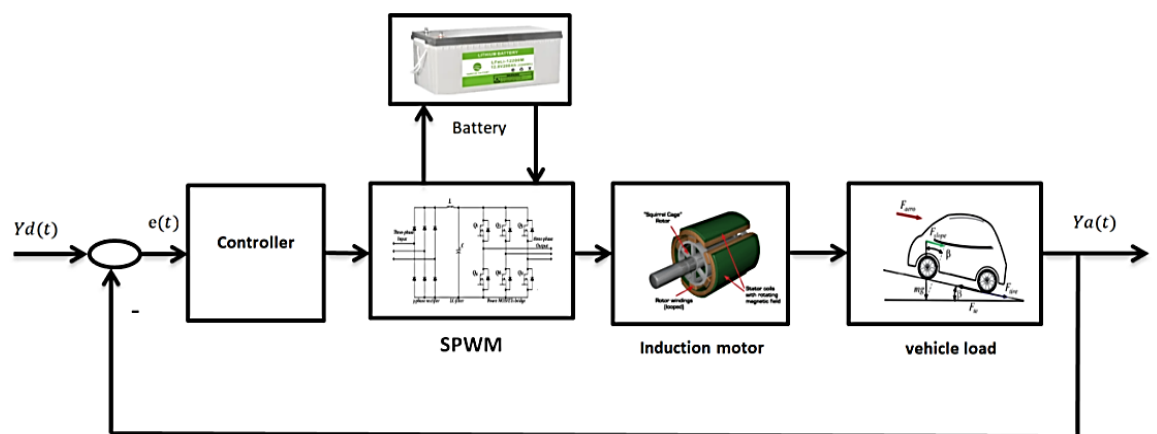

Figure 1. Block diagram of electrical traction chain

2.1. Energy source

For the purposes of this study, the simplified model takes into account the key characteristics of the lithium-ion battery, such as its voltage, current, and capacity. The sophisticated battery model described in has been modified [17]. By using this simplified model, we aim to gain a better understanding of the behavior and limitations of the lithium-ion accumulator battery in practical applications.

2.2. SPWM Inverter

An inverter controls the power frequency of an AC motor in order to control the motor's rotational speed. In the absence of an inverter, the AC motor would begin to run at full speed as soon as the power source was turned on. Circuits for power electronic inverters commonly use sinusoidal pulse width modulation (SPWM), a widely used control method. It offers advantages like low switching losses, a cleaner output, and ease of usage. Sinusoidal pulse width modulation (SPWM) is the AC driving technique that is most frequently employed. This suggests that it should have a stiff source at its input and a voltage source inverter (VSI) at its output [18]. Each power bridge device, which consists of two power switches and two freewheeling diodes, has three outputs in a practical (VSI). The inverter gets electricity from a DC voltage source via an LC filter. As seen in Figure 2, the three output legs of SPWM can be thought of as three distinct push-pull amplifiers.

By first producing a carrier triangle signal and three modulating signals to determine the angular speed ($\omega_e t$), and then by comparing the two signal sets to produce switching signals for three push-pull devices. When the switches' output is (V_{ao}, V_{bo}, V_{co}), the three phases of the load neutral (V_{an}, V_{bn}, V_{cn}) can be obtained by implementing (1).

$$\begin{bmatrix} V_{an} \\ V_{bn} \\ V_{cn} \end{bmatrix} = \frac{1}{2} \begin{bmatrix} 2 & -1 & -1 \\ -1 & 2 & -1 \\ -1 & -1 & 2 \end{bmatrix} \begin{bmatrix} V_{ao} \\ V_{bo} \\ V_{co} \end{bmatrix} \tag{1}$$
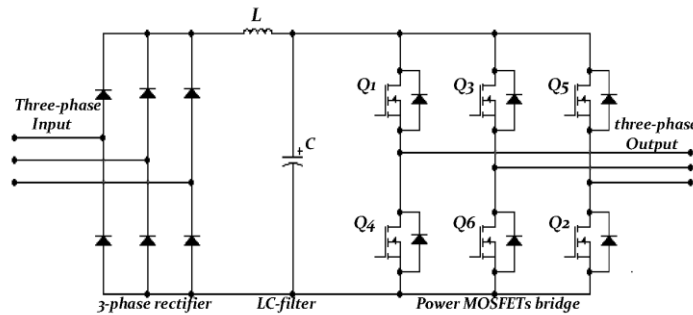

Figure 2. Three phase voltage source inverter

2.3. Traction motor

The motor in use is a three-phase induction motor (IM) with sinusoidal pulse width modulation (SPWM) control, powered by a voltage inverter. One of the most well-known induction motor models created from its equivalent circuit is Krause's model, which is based on a transformation of the stator's currents and magnetic fluxes to a reference frame "d-q" that rotates in tandem with the rotor [19]. The three-phase parameters (voltage, current, and flux) are transmitted via axis transformation, and as the rotor position varies, the coupling coefficients between the stator and rotor phases change continuously (d-q axes stationary frame). The rate of rotation of the rotor and stator, as well as the acceptance of all simulated variables in the stationary frame to account DC values [20]. Figure 3 shows schematics of an I.M.'s per-phase equivalent circuits in a two-axis synchronously rotating reference frame.

In Figure 3 "$\Psi_{ds} \Psi_{qs}$", "$\Psi_{dr}\Psi_{qr}$" d-q axes elements flux linkage of the stator and rotor. "$V_{ds} V_{qs}$", "$V_{dr}V_{qr}$" d-q axes elements stator voltage, rotor voltage, " ,"$i_{ds} i_{qs}$" and "$i_{dr}i_{qr}$" stator current and rotor current respectively. "L_{sl}, L_{rl}" Stator and rotor inductance. "$R_s R_r$" Stator and rotor winding resistance. w_r Rotor speed. L_m Magnetizing inductance. "w_e" Synchronous speed. From the figure we can get the (2) and (3) [17]:

$$\frac{d}{dt} \begin{bmatrix} \Psi_{qs} \\ \Psi_{ds} \\ \Psi_{qr} \\ \Psi_{dr} \end{bmatrix} = \begin{bmatrix} 0 & -w_e & 0 & 0 \\ -w_e & 0 & 0 & 0 \\ 0 & 0 & 0 & w_r - w_e \\ 0 & 0 & w_r - w_e & 0 \end{bmatrix} \begin{bmatrix} \Psi_{qs} \\ \Psi_{ds} \\ \Psi_{qr} \\ \Psi_{dr} \end{bmatrix} + \begin{bmatrix} V_{qs} - R_s i_{qs} \\ V_{ds} - R_s i_{ds} \\ V_{qr} - R_r i_{qr} \\ V_{dr} - R_r i_{dr} \end{bmatrix} \tag{2}$$

$$\begin{bmatrix} \Psi_{qs} \\ \Psi_{ds} \\ \Psi_{qr} \\ \Psi_{dr} \end{bmatrix} = - \begin{bmatrix} L_{sl} + L_m & 0 & L_m & 0 \\ 0 & L_{sl} + L_m & 0 & L_m \\ L_m & 0 & L_{sl} + L_m & 0 \\ 0 & L_m & 0 & L_{sl} + L_m \end{bmatrix} \begin{bmatrix} i_{qs} \\ i_{ds} \\ i_{qr} \\ i_{dr} \end{bmatrix} \tag{3}$$

The development torque T_e can be calculated using the (4) by combining the effects of the air gap flux and rotor current I_r and solving the variables into a stationary frame with dq-axes.

$$T_e = \left(\frac{3}{2}\right)\left(\frac{p}{2}\right)\left(\Psi_{dr} i_{qr} - \Psi_{qr} i_{dr}\right) \tag{4}$$

It is formed in (5) that the dynamic torque equation of the rotor where T_L is the electric vehicle load torque and J is the rotor's inertia [21].

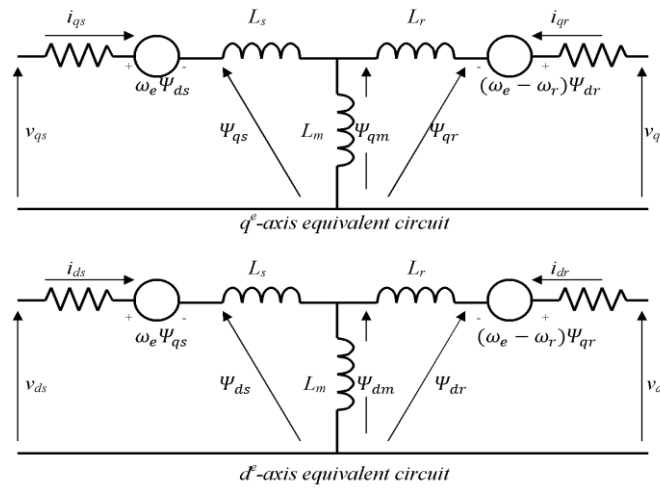$$T_e = T_L + \left(\frac{2}{p}\right) J \frac{dw_r}{dt} \tag{5}$$

Figure 3. IM equivalent circuit is d-q axes elements

2.4. Mathematical model of vehicle load

Figure 4 shows an electric vehicle that is in equilibrium with respect to all of the forces acting on it while it is moving. Balancing and optimizing these forces are crucial for the efficiency and performance of electric vehicles. Manufacturers and designers must consider these forces to enhance the vehicle's energy efficiency and overall performance.

2.4.1. Aerodynamic force

These forces shown in Figure 4 are resulted from body friction of the vehicle with the inclined path as well as air. They are functions of the protrusion of the frontal shape area such as mirrors, sides, ducts and any other factors. The component as shown in (6).

$$F_{areo} = \frac{1}{2} \rho A C_d v^2 \tag{6}$$

2.4.2. Rolling force

The tire's traction on the road results in what is called rolling resistance, which is primarily caused by. Other factors generating friction are the bearing and gearing systems that play a role in this matter. Rolling force resistance is nearly constant and proportional to vehicle weight, depending on vehicle speed. This force can be represented (including the above affecting factors) as in (7).

$$F_{tire} = \mu_{rr} mg \tag{7}$$

2.4.3. Hill climbing force

The most needed force to find is the driving force of the vehicle up (climbing force), in which it is a combination of the weight of the vehicle acting along the slop. However, this force can be represented as (8) [22].

$$F_{slope} = mgsin(\beta) \tag{8}$$

The fourth force also affected that is called acceleration force as show in (9).

$$F_{acce} = \frac{mdv}{dt} \tag{9}$$

We obtain finally the total forces effected on the electrical vehicle as show in (10).

$$F = \frac{1}{2}\rho AC_d v^2 + \mu_{rr}mg + mgsin(\beta) + \frac{mdv}{dt} \tag{10}$$

Where v denotes the velocity of the EV, A denotes the head of the vehicle or truck, m denotes the mass of the electrical vehicle, μ_{rr} denotes the rolling resistance coefficient, g denotes the acceleration of gravity, ρ denotes air density, and β denotes the angle at which the machine climbs a slope, or the climbing angle, and last but not least, C_d denotes the coefficient of the drag operation.

As shown by (11) [23], the consequence of the force (F), which is a torque, will provide a result that is unfavorable to the motor that is doing the driving.

$$T_L = F\left(\frac{r}{G}\right) \tag{11}$$

Where G stands for the gearing ratio and r for the radius of the electric vehicle tires. Additionally, T_L is used to signify the torque that the EV driving motor will deliver.
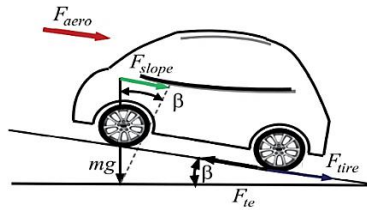

Figure 4. The action of forces on a moving vehicle on inclined road [24]

3.   THE ROBUST INTEGRAL SIGNUM OF THE ERROR CONTROLLER

The robust integral signum of the error controller (RISE) is suggested in [25], it is used with an unknown nonlinear system. Using the integral signum of the error distinguishes the RISE control system from first order sliding mode control. This concept allows for asymptotic monitoring and prevents chattering plague in traditional sliding mode controllers [26]. What distinguishes the RISE controller only the error is required for constructing it (the mismatch between the system's output and its reference points tracking). Despite external disruptions and modeling errors, the goal of the control method is to guarantee that the actual output, $Ya(t)$ tracing the desired signal $Yd(t)$. The difference between the two signals is given by (12).

$$e(t) = Y_d(t) - Y_a(t) \tag{12}$$

The main objective of control is to provide a continuous robust control law that ensures the error (the difference between the planned input and the actual output) asymptotically converges to zero, is $|e1| \rightarrow 0$ as $t \rightarrow 0$. Auxiliary error signals, represented by the notation $ei \in R$ where $i = 1, .. n$ the superscript n denotes the order of the system. For the three-phase electric vehicle, where n=2, the auxiliary error is defined in (13) and (14) as [27]:

$$e_1(t) = k_1\left(Y_d(t) - Y_a(t)\right) \tag{13}$$

$$e_2(t) = k_2 e_1(t) + \dot{e}_1(t) \tag{14}$$

So, the auxiliary error signal is given by [28]. Then, the RISE controller is given by following control signal (15) [29].

$$u(t) = (k_a + 1)\left[e_2(t) - e_2(t_o) + \sigma \int_0^t e_2(\sigma)\,d\sigma\right] + \int_0^t \beta * sat\left(e_2(\sigma)\right)d\sigma \tag{15}$$

Where the normal saturation function is sat(.) and the controller parameters are $k_1, k_2, k_a, \sigma, \beta \in R$, these parameters are determined by SSA, which will be detailed in the next section. To guarantee that $u(t_o) = 0$, the $e_2(t_o)$ term was applied.

4. SALP SWARM ALGORITHM (SSA)

The SSA is a meta-heuristic method that Mirjalili and colleagues recently proposed in 2017 [30]. It takes its cues from the way salps swarm together in the ocean. Using the stochastic method SSA, a population of initial random solutions is created, and to start the optimization process, this population is then improved over time through two stages—exploring and exploiting. In the first stage, the search space is investigated to find the most promising areas. In the second stage, better solutions are discovered by looking in the general area of unusual solutions. The random population (salp) division divides the salp chains mathematically into two classes. In a group of salps, the first salp is referenced as the leader, while the following salps are referenced as followers. To update the leader's position, apply (16)-(17).

$$X_j^1 = \begin{cases} F_j + c_1\left(\left(ub_j - lb_j\right) * c_2 + lb_j\right) \ if \ c_3 \leq 0.5 \\ F_j - c_1\left(\left(ub_j - lb_j\right) * c_2 + lb_j\right) \ if \ c_3 > 0.5 \end{cases} \tag{16}$$

$$c_1 = 2e^{-(\frac{4t}{T})^2} \tag{17}$$

For updating the followers' location, (18) (Newton movement law) is used.

$$X_j^i = \frac{1}{2}\left(X_j^i + X_j^{i-1}\right) \tag{18}$$

Where X_j^1 and X_j^i represent the leader and followers' positions in the jth dimension, respectively, and $i \geq 2$. The food supply locations in the j-th dimension are represented by F_j. The parameters c_2 and c_3 are distributed at random within the range [0 1]. The symbols ub_j and lb_j stand for the upper and lower boundaries of the search space in the j-th dimension. The letter t stands for the current iteration. The maximum number of iterations is considered to be T [31]. The integral time squared error (ITSE) (integral time-weighted squared error) is the cost function employed in this study and is given by (19).

$$Fitness = \ ITSE = \int_0^t t * e(t)^2 \tag{19}$$

Where e(t) represents the difference in EV speed between the desired input and the actual speed.

5. RESULTS AND DISCUSSION

Utilizing the MATLAB 2020a program, simulations of the proposed ORISE controller in comparison to PID are run. A PC running Windows 10 with a Core i7 processor clocked at 2.40 GHz and 8 GB of RAM is used for this. The control system simulated in MATLAB/Simulink, the parameters of the SSA that achieve better solution for both ORISE and PID are listed in Table 1. Fixed linear and bang-bang trajectories are used to test the overall controlled system. Table 2 lists the ORISE and PID controller's tuned parameters by SSA.

5.1. Simulation results of the fixed linear trajectory

To assess the step responsiveness of the entire system (the EV controlled by ORISE controller compared to PID based on SSA), a fixed input signal is employed. Figure 5 displays the simulation results, and Table 3 summarizes the time response criteria. These results show that the PID controller based on SSA that suffer from chattering and has higher oscillation (maximum overshot $M_P > 5\%$), compared with ORISE controller that improved speed response and minimum or no oscillation (maximum peak $M_P < 2\%$). Figures 6 and 7, respectively, display the ORISE and PID control signals.

Figures 8 show the torque load responses of comparison between PID and ORISE controller. The starting torque is large when compared with the steady state condition, which is needed to overcome the motor inertia before the speed reach to the reference value. The electromagnetic torque is related to the load torques with ripple as shown in figures.

5.2. Simulation results of bang-bang linear trajectory

In Figure 9 the test's outcomes are shown. The outcomes demonstrate that the two proposed controllers are precise and quick to react while tracking the vehicle's speed to the intended speed, however the PID controller also suffers from chattering, making the system unstable in comparison to the ORISE controller which makes the system stable. The findings for both linear and nonlinear courses produced show how effective the suggested ORISE controllers are at driving an electric vehicle.

The outcomes of the tests mentioned above showed that the suggested ORISE controller is suitable for usage as an EV controller. It has the ability to deal with input changes of any kind, including rapid sharp changes. This is due to the fact that the suggested controller's dependability in controlling the induction-motor for various input types is confirmed by its extremely short rising time, settling time, and modest steady-state error.

Table 1. The parameters of SSA algorithms for two controllers

Parameters of SSA	PID controller	RISE controller
No. of iterations (N_i)	50	50
No. of search agents/universes (n)	10	5
No. of variables (Dim)	3	5
Lower bound (lb)	[10 5 0.1]	[1 1 1 1 1]
Upper bound (ub)	[40 15 10]	[10 10 10 10 10]

Table 2. The optimal parameters of the two controllers

PID parameters	Values	RISE parameters	Values
K_p	21.4207	k_1	6
K_i	2.6969	k_2	2.2276
K_d	1.4351	k_a	2.3344
		σ	5.1867
		β	7.4657

Table 3. Comparison between the performances of ORISE and PID controllers

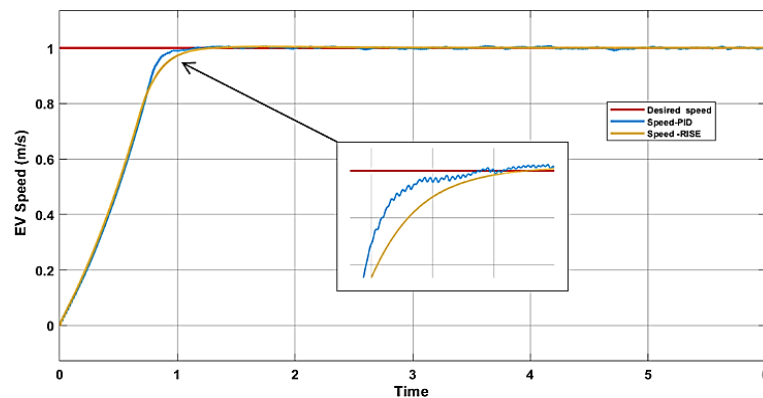| Speed controller	Maximum overshoot M_P (%)	Delay time t_d(sec)	Peak time t_p(sec)	settling time t_S (sec.)	rising time t_r (sec.)	steady state error
PID-SSA	0.05	0.504	1.312	1.532	0.785	0.005
RISE-SSA	0.002	0.491	1.574	1.915	0.821	0.002

Figure 5. Speed response with ORISE and PID based on SSA
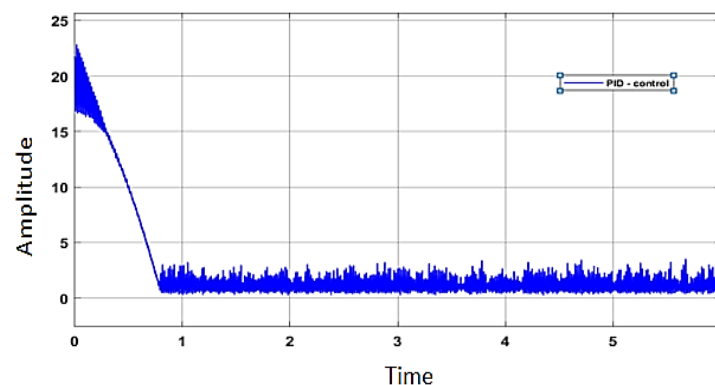
Figure 6. The control signal of PID for linear path

Design an optimal robust integral signum of the error controller for electrical vehicle ... (Arkan A. Jassim)
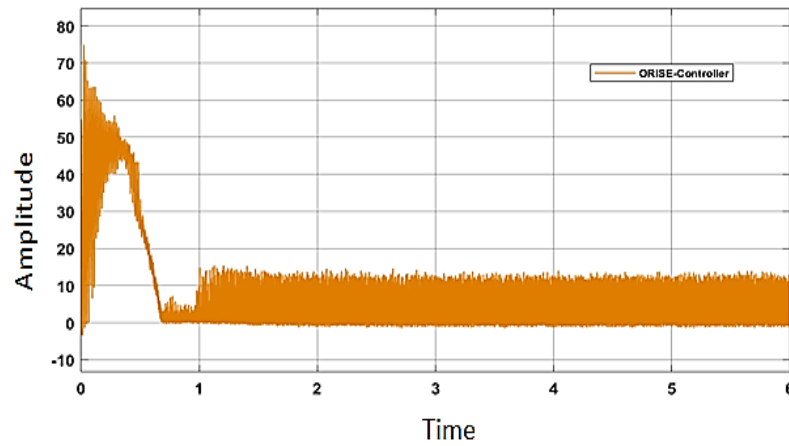
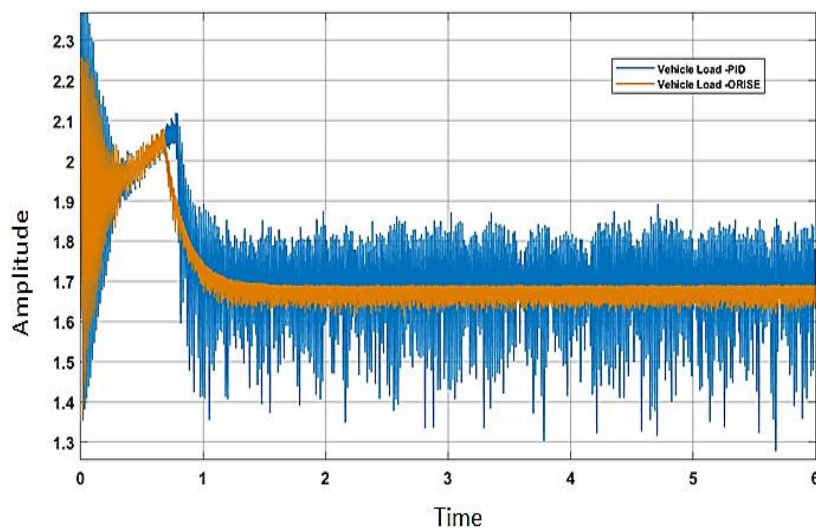Figure 7. The control signal of ORISE for linear path

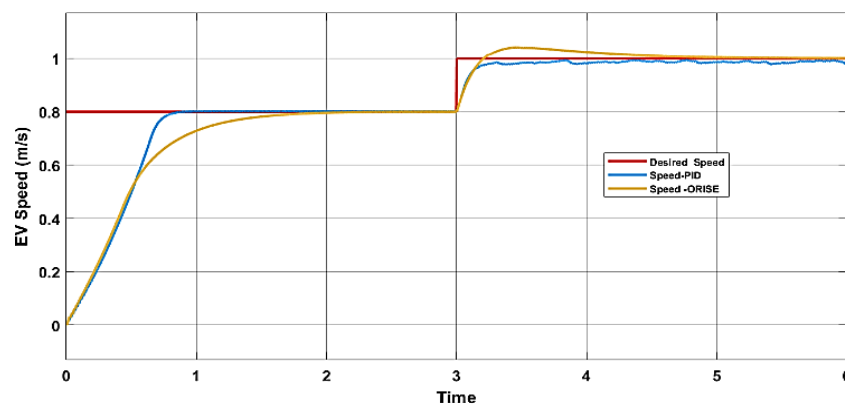Figure 8. Torque load vehicle responses of comparison between ORISE and PID controller

Figure 9. Speed response with ORISE and PID controllers with SSA optimization

6. CONCLUSION

In this paper a control system of electric vehicle using 3-Phase VSI and SPWM is developed and simulated in MATLAB-Simulink. An optimal RISE based on SSA is demonstrated in this paper. a technique is used to provide a more reliable controller for this system (with accurate speed tracking and minimal lag);

the controlled speed of the electric vehicle based on the ORISE controller is more closely with desired input speed than PID controller. with high accuracy either in flat roads or curved. In this work, The simulation results of the fixed linear trajectory test it has been shown that ORISE controllers perform better than PID controller because they showed lower overshoot but PID lower in rising time. The project can be extended further in the future by switching out the induction motor for another motor for the electric vehicle system, such as a switched reluctance motor, brushless DC motors, etc. It can also be implemented using FPGA technology or any other technology.

REFERENCES

[1]   J. A. P. Lopes, F. J. Soares, P. M. R. Almeida, P. C. Baptista, C. M. Silva, and T. L. Farias, "Quantification of technical impacts and environmental benefits of electric vehicles integration on electricity grids," in *2009 8th International Symposium on Advanced Electromechanical Motion Systems & Electric Drives Joint Symposium*, Jul. 2009, pp. 1–6, doi: 10.1109/ELECTROMOTION.2009.5259139.

[2]   R. Sioshansi and P. Denholm, "Emissions impacts and benefits of plug-in hybrid electric vehicles and vehicle-to-grid services," *Environmental Science and Technology*, vol. 43, no. 4, pp. 1199–1204, Feb. 2009, doi: 10.1021/es802324j.

[3]   S. M. Lukic and A. Emadi, "Effects of drivetrain hybridization on fuel economy and dynamic performance of parallel hybrid electric vehicles," *IEEE Transactions on Vehicular Technology*, vol. 53, no. 2, pp. 385–389, 2004, doi: 10.1109/TVT.2004.823525.

[4]   S. Englberger, H. Hesse, D. Kucevic, and A. Jossen, "A techno-economic analysis of vehicle-to-building: Battery degradation and efficiency analysis in the context of coordinated electric vehicle charging," *Energies*, vol. 12, no. 5, p. 955, Mar. 2019, doi: 10.3390/en12050955.

[5]   F. Un-Noor, S. Padmanaban, L. Mihet-Popa, M. N. Mollah, and E. Hossain, "A comprehensive study of key electric vehicle (EV) components, technologies, challenges, impacts, and future direction of development," *Energies*, vol. 10, no. 8, p. 1217, Aug. 2017, doi: 10.3390/en10081217.

[6]   A. Arancibia, K. Strunz, and F. Mancilla-David, "A unified single- and three-phase control for grid connected electric vehicles," *IEEE Transactions on Smart Grid*, vol. 4, no. 4, pp. 1780–1790, Dec. 2013, doi: 10.1109/TSG.2013.2271096.

[7]   M. Vasudevan and R. Arumugam, "New direct torque control scheme of induction motor for electric vehicles," *2004 5th Asian Control Conference*, vol. 2, pp. 1377–1383, 2004.

[8]   L. Baghli, "Contribution to induction machine control: Using fuzzy logic, neural networks and genetic algorithms," Henri Poincare University, 1999.

[9]   M. A. Ouhrouche and C. Volat, "Simulation of a direct field-oriented controller for an induction motor using MATLAB/Simulink software package ξ α," in *Proceedings of the IASTED International Conference MS'2000*, 2000, no. 1, pp. 15–17.

[10]   J. Jung and K. Nam, "A dynamic decoupling control scheme for high-speed operation of induction motors," *IEEE Transactions on Industrial Electronics*, vol. 46, no. 1, pp. 100–110, 1999, doi: 10.1109/41.744397.

[11]   N. Stefanovic, "Robust L2 nonlinear control of EDFA with amplified spontaneous emission," University of Toronto, 2005.

[12]   A. Nasri, B. Gasbaoui, and B. M. Fayssal, "Sliding mode control for four wheels electric vehicle drive," *Procedia Technology*, vol. 22, pp. 518–526, 2016, doi: 10.1016/j.protcy.2016.01.111.

[13]   T. Pourseif and M. Mohajeri, "Design of robust control for a motor in electric vehicles," *IET Electrical Systems in Transportation*, vol. 10, no. 1, pp. 68–74, 2020, doi: 10.1049/iet-est.2018.5084.

[14]   M. Zand, M. Azimi Nasab, M. Khoobani, A. Jahangiri, S. Hossein Hosseinian, and A. Hossein Kimiai, "Robust speed control for induction motor drives using STSM control," in *2021 12th Power Electronics, Drive Systems, and Technologies Conference, PEDSTC 2021*, Feb. 2021, pp. 1–6, doi: 10.1109/PEDSTC52094.2021.9405912.

[15]   X. Jin, J. Wang, S. Sun, S. Li, J. Yang, and Z. Yan, "Design of constrained robust controller for active suspension of in-wheel-drive electric vehicles," *Mathematics*, vol. 9, no. 3, pp. 1–16, 2021, doi: 10.3390/math9030249.

[16]   Y. Hori, Y. Toyoda, and Y. Tsuruoka, "Traction control of electric vehicle: Basic experimental results using the test EV UOT electric march," *IEEE Transactions on Industry Applications*, vol. 34, no. 5, pp. 1131–1138, 1998, doi: 10.1109/28.720454.

[17]   S. Sadeghi, J. Milimonfared, M. Mirsalim, and M. Jalalifar, "Dynamic modeling and simulation of a switched reluctance motor in electric vehicles," in *2006 1st IEEE Conference on Industrial Electronics and Applications*, May 2006, pp. 1–6, doi: 10.1109/ICIEA.2006.257348.

[18]   O. Anaya-Lara, N. Jenkins, J. B. Ekanayake, P. Cartwright, and M. Hughes, *Wind energy generation: modelling and control*. John Wiley & Sons, 2011.

[19]   B. Ozpineci and L. M. Tolbert, "Simulink implementation of induction machine model - a modular approach," in *IEEE International Electric Machines and Drives Conference, 2003. IEMDC'03.*, 2003, vol. 2, pp. 728–734, doi: 10.1109/IEMDC.2003.1210317.

[20]   G. G. Rigatos, "Modelling and control for intelligent industrial systems," *The effects of brief mindfulness intervention on acute pain experience: An examination of individual difference*, vol. 7, pp. 1689–1699, 2011, [Online]. Available: http://link.springer.com/10.1007/978-3-642-17875-7.

[21]   Aidi Shen, Hui Huang, and Wei Kang, "Marine AC high-capacity drive experiment system," in *2010 International Conference on Computer, Mechatronics, Control and Electronic Engineering*, Aug. 2010, vol. 3, pp. 33–36, doi: 10.1109/CMCE.2010.5610412.

[22]   M. E. H. Benbouzid, D. Diallo, and M. Zeraoulia, "Advanced fault-tolerant control of induction-motor drives for EV/HEV traction applications: From conventional to modern and intelligent control techniques," *IEEE Transactions on Vehicular Technology*, vol. 56, no. 2, pp. 519–528, 2007, doi: 10.1109/TVT.2006.889579.

[23]   M. H. Khooban, N. Vafamand, and T. Niknam, "T–S fuzzy model predictive speed control of electrical vehicles," *ISA Transactions*, vol. 64, pp. 231–240, Sep. 2016, doi: 10.1016/j.isatra.2016.04.019.

[24]   M. H. Khooban, N. Vafamand, T. Niknam, T. Dragicevic, and F. Blaabjerg, "Model-predictive control based on Takagi-Sugeno fuzzy model for electrical vehicles delayed model," *IET Electric Power Applications*, vol. 11, no. 5, pp. 918–934, May 2017, doi: 10.1049/iet-epa.2016.0508.

[25]   B. Xian, D. M. Dawson, M. S. de Queiroz, and J. Chen, "A continuous asymptotic tracking control strategy for uncertain nonlinear systems," *IEEE Transactions on Automatic Control*, vol. 49, no. 7, pp. 1206–1211, 2004, doi: 10.1109/TAC.2004.831148.

[26]   B. Bidikli, E. Tatlicioglu, A. Bayrak, and E. Zergeroglu, "A new robust 'integral of sign of error' feedback controller with adaptive compensation gain," in *Proceedings of the IEEE Conference on Decision and Control*, Dec. 2013, pp. 3782–3787, doi: 10.1109/CDC.2013.6760466.

[27]   A. J. N. Anelone, M. F. Villa-Tamayo, and P. S. Rivadeneira, "Oncolytic virus therapy benefits from control theory," *Royal Society Open Science*, vol. 7, no. 7, p. 200473, Jul. 2020, doi: 10.1098/rsos.200473.

[28]　L. Li, S. Liu, D. Han, B. Tang, and J. Ma, "Delivery and Biosafety of Oncolytic Virotherapy," *Frontiers in Oncology*, vol. 10, Apr. 2020, doi: 10.3389/fonc.2020.00475.

[29]　P.-H. Kim *et al.*, "Active targeting and safety profile of PEG-modified adenovirus conjugated with herceptin," *Biomaterials*, vol. 32, no. 9, pp. 2314–2326, Mar. 2011, doi: 10.1016/j.biomaterials.2010.10.031.

[30]　S. Mirjalili, A. H. Gandomi, S. Z. Mirjalili, S. Saremi, H. Faris, and S. M. Mirjalili, "Salp swarm algorithm: A bio-inspired optimizer for engineering design problems," *Advances in Engineering Software*, vol. 114, pp. 163–191, Dec. 2017, doi: 10.1016/j.advengsoft.2017.07.002.

[31]　J. Wu, R. Nan, and L. Chen, "Improved salp swarm algorithm based on weight factor and adaptive mutation," *Journal of Experimental and Theoretical Artificial Intelligence*, vol. 31, no. 3, pp. 493–515, 2019, doi: 10.1080/0952813X.2019.1572659.

BIOGRAPHIES OF AUTHORS

Arkan A. Jassim was born in Dyala, Iraq in 1993. He obtained a bachelor's degree in electronic engineering from the University of Mosel, Iraq in 2016. He obtained a master's degree in electronics and communication engineering from University of Technology, Iraq in 2019. Currently, he studies a Ph.D. in University of Technology, his research of interests is mainly in controller, power electronic and artificial intelligent. He can be contacted at email: arkan199328@gmail.com.

Ekhlas H. Karam got Ph.D. degree from University of Technology, Baghdad, Iraq in 2007. She is academic staff member in Computer Engineering Department at Al-Mustansirya University. Her intereste area is robotic system, intellgent systems controller design, optimization methods, control design by FPGA. She can be contacted at email: ekkaram2020@gmail.com.

Mohammed Moanes E. Ali was born in Baghdad, Iraq in 1971. He received the B.Sc., M.Sc., and Ph.D. degrees in electrical engineering from University of Technology, Iraq in 1994, 1997, and 2009, respectively. Since May 2006, he has been with the Department of Electrical Engineering-University of Technology, where he was an assistance lecture. He became a lecturer in 2009, and an assistance professor in 2018. His current research interests include electro heat (induction heating), electrical machines, and drives. He published more than 32 technical papers. He can be contacted at email: mohammedmoanes.e.ali@uotechnology.edu.iq.